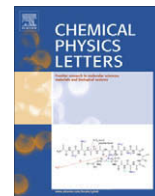




Contents lists available at ScienceDirect

Chemical Physics Letters

journal homepage: www.elsevier.com/locate/cplett

Ab initio study of coherent anti-Stokes Raman scattering (CARS) of the 1,3,5-trinitro-1,3,5-triazacyclohexane (RDX) explosive

Abdelsalam Mohammed^{a,*}, Hans Ågren^a, Andreas J. Thorvaldsen^b, Kenneth Ruud^b

^aTheoretical Chemistry, Royal Institute of Technology, SE-100 44 Stockholm, Sweden

^bCentre for Theoretical and Computational Chemistry, Department of Chemistry, University of Tromsø, N-9037 Tromsø, Norway

ARTICLE INFO

Article history:

Received 24 November 2009

In final form 22 December 2009

Available online xxxxx

ABSTRACT

Coherent anti-Stokes Raman scattering (CARS) of the 1,3,5-trinitro-1,3,5-triazacyclohexane (RDX) $C_3H_6N_6O_6$ molecule is studied by *ab initio* methods. The results are compared to available experimental observations and against calculations and experimental observations of the conventional non-resonant Raman spectrum for RDX. It is found that all intense bands in the observed CARS spectrum and all Raman differential cross sections are well reproduced by the calculations. The features of the resonant CARS signal vary strongly from the corresponding Raman signal, and are obtained with a considerably larger cross section, a fact that could further facilitate the use of CARS spectroscopy in applications of stand-off detection of gaseous samples at ultra-low concentrations.

© 2009 Elsevier B.V. All rights reserved.

1. Introduction

Raman spectroscopy is a widely used technique in areas such as chemical and material science, art restoration, gemology, as well as in military and biomedical applications. A major limitation of Raman spectroscopy is, however, that the Raman effect is extremely weak and requires high average laser power to compensate for the low scattering cross sections which often, at resonance conditions, can suffer from the presence of a fluorescence background [1,2]. These difficulties can be circumvented by the application of a multiphoton technique based on coherent anti-Stokes Raman scattering (CARS) [1]. Advances in recent years have turned this technique into a unique and powerful tool used worldwide to probe structure and function of molecular or composite materials in biology, neurobiology, pathology, and pharmacology [2]. In the biomedical area, CARS makes it possible to perform imaging of plant cells and tissue, and the technique also provides exciting possibilities for gaining information on processes at the microscopic scale [2,3]. Additional advantages of CARS for biological applications is its high energy conversion, its insensitivity towards fluorescence and its excellent time resolution [4]. Many opportunities for pushing the fundamental limits of CARS microscopy continue to be unravelled [2,5–8].

CARS microscopy is also expected to have potential applications in the field of stand-off detection of foreign substances in gaseous form or in interaction with substrates [9]. Operation at ultra-low

intensities is most often required in order to detect single molecules or microscopic objects for which the basic Raman cross section generally is very small. As such, CARS may be a more attractive alternative to conventional Raman spectroscopy for obtaining vibrationally resolved fingerprint spectra of fluorescing molecules [4,10].

CARS originates in a third-order nonlinear optical process which utilizes two relatively high-powered laser beams, where a pump and a Stokes laser beam, with angular frequencies ω_p and ω_s , are focused into a sample. Due to the laser mixing, a coherent beam resembling a low intensity laser beam at the anti-Stokes frequency of $\omega_{as} = 2\omega_p - \omega_s$ is generated in the medium [11]. The CARS signal is significantly enhanced when $\omega_p - \omega_s$ coincides, or is tuned to be, resonant with a molecular vibration ω_v . Despite the fact that CARS nowadays is a widely used technique with a well established theoretical foundation, *ab initio* studies of CARS spectra of molecular systems have been lacking. This state of affairs was very recently resolved when Thorvaldsen et al. [12] presented a formalism that allows for fully analytical calculations of CARS spectra. The formalism is a special case of an open-ended theory for the calculation of frequency-dependent molecular response properties of arbitrary order, including also contributions from perturbation-dependent basis sets, and formulated fully in the atomic-orbital basis [13]. The applicability of the theory was demonstrated by calculations on a set of polyaromatic hydrocarbons. The work of Thorvaldsen et al. opens for new possibilities for practical applications of CARS, as it lends itself to the design of CARS labels and also *a priori* identification of CARS fingerprints in label-free probes. Furthermore, the ability to make precise determination of absolute CARS cross sections makes it possible to predetermine the requirements for

* Corresponding author.

E-mail addresses: Abdelsalam.M.Mohammed@gmail.com, salam@theochem.kth.se (A. Mohammed).

technical parameters in measurements, for instance for the lasers and detectors at any given geometrical setup in a stand-off detection. In order to illustrate and confirm these new possibilities, we will in this work apply the method to calculate the CARS spectrum of a common explosive molecule of interest in stand-off detection technology, namely 1,3,5-trinitro-1,3,5-triazacyclohexane (RDX) $C_4H_6N_6O_6$. We compare the computed CARS with non-resonant Raman spectra, which is the conventionally applied methodology. We also present calculations of the two spectroscopies on benzonitrile C_7H_5N (BN), which has a well-characterized CARS spectrum, thus serving as a good test case for our methodological approach.

2. Theory and methodological approach

2.1. Coherent anti-Stokes Raman scattering

The Coherent anti-Stokes Raman Scattering (CARS) process is formally a four-wave mixing process in which two of the frequencies are the same [14]. The observed CARS signal is thus related to the fourth-order susceptibility tensor $\chi^{(3)}(-\omega_\sigma; \omega_1, -\omega_2, \omega_1)$, where the sign of the frequency ω_2 is negative since it corresponds to a deexcitation (the Stokes signal). The outgoing CARS signal is given as $\omega_\sigma = 2\omega_1 - \omega_2$. At the microscopic level, the susceptibility tensor is governed by the second hyperpolarizability tensor, which in the general case can be written as [15]:

$$\begin{aligned} \gamma_{\alpha\beta\gamma\delta}(-\omega_\sigma; \omega_1, \omega_2, \omega_3) = & \frac{1}{\hbar^3} \sum \mathcal{P}_{1,2,3} \\ & \times \sum_{nmp} \left[\frac{\langle 0|\hat{\mu}_\alpha|n\rangle\langle n|\hat{\mu}_\beta|m\rangle\langle m|\hat{\mu}_\gamma|p\rangle\langle p|\hat{\mu}_\delta|0\rangle}{(\omega_{n0} - \omega_\sigma - i3\epsilon)(\omega_{m0} - \omega_2 - \omega_3 - i2\epsilon)(\omega_{p0} - \omega_3 - i\epsilon)} \right. \\ & + \frac{\langle 0|\hat{\mu}_\beta|n\rangle\langle n|\hat{\mu}_\alpha|m\rangle\langle m|\hat{\mu}_\gamma|p\rangle\langle p|\hat{\mu}_\delta|0\rangle}{(\omega_{n0} + \omega_1 + i\epsilon)(\omega_{m0} - \omega_2 - \omega_3 - i2\epsilon)(\omega_{p0} - \omega_3 - i\epsilon)} \\ & + \frac{\langle 0|\hat{\mu}_\gamma|m\rangle\langle m|\hat{\mu}_\beta|n\rangle\langle n|\hat{\mu}_\alpha|p\rangle\langle p|\hat{\mu}_\delta|0\rangle}{(\omega_{n0} + \omega_1 + \omega_2 + i2\epsilon)(\omega_{m0} + \omega_2 + i\epsilon)(\omega_{p0} - \omega_3 - i\epsilon)} \\ & \left. + \frac{\langle 0|\hat{\mu}_\delta|p\rangle\langle p|\hat{\mu}_\gamma|m\rangle\langle m|\hat{\mu}_\beta|n\rangle\langle n|\hat{\mu}_\alpha|0\rangle}{(\omega_{n0} + \omega_\sigma + i3\epsilon)(\omega_{m0} + \omega_2 + \omega_3 + i2\epsilon)(\omega_{p0} + \omega_3 + i\epsilon)} \right]. \end{aligned} \quad (1)$$

In the expression given above, $\mathcal{P}_{1,2,3}$ permutes the operators and their corresponding frequencies, and we have introduced the α component of the electric dipole operator $\hat{\mu}_\alpha$ and $\hbar\omega_{n0}$ as the excitation energy from the ground $|0\rangle$ to the excited state $|n\rangle$. $\hbar\omega_1$ is the energy per photon of the incoming light, and $i\epsilon$ is introduced to avoid divergencies when the denominators go to zero. However, $i\epsilon$ may be given a physical interpretation as representing the finite lifetime of the vibrationally excited states, and thus describe the absorption processes that occur close to electronic or vibrational resonances. The summations in the above equations run over all possible vibronic states.

In a molecule, there are multiple sources of the second hyperpolarizability tensor that determines the CARS intensities, such as for instance the second electronic hyperpolarizability (in which all the excited states in the summations in Eq. (1) correspond to electronically excited states), as well as various non-resonant pure vibrational effects [16]. However, the dominating signals arise when the pump beam ω_1 and the Stokes signal ω_2 matches a vibrational excitation in the molecule $\omega_1 - \omega_2 \approx \omega_{k0}$, with $\hbar\omega_{k0}$ corresponding to the excitation energy of a vibrational mode in the molecule. The CARS process thus in principle has the same information content as conventional off-resonant Raman spectroscopy, but with a much higher intensity (up to five orders of magnitude). As the process in general generates an anti-Stokes signal, blue-shifted with respect to the incoming laser (s), the process is also less susceptible to fluorescence in the sample.

The dominating resonant contribution to the CARS signal can be shown to be given by [12,14]

$$\begin{aligned} \gamma_{\alpha\beta\gamma\delta}^{\text{CARS,Res}}(-\omega_\sigma; \omega_1; -\omega_2, \omega_1) \approx & \frac{2}{\hbar} \sum_k \left[\frac{\langle 0|\alpha_{\alpha\beta}(\omega_1)|k\rangle\langle k|\alpha_{\gamma\delta}(\omega_1)|0\rangle}{\omega_{k0} - (\omega_1 - \omega_2) + i2\epsilon} \right. \\ & \left. + \frac{\langle 0|\alpha_{\alpha\delta}(\omega_1)|k\rangle\langle k|\alpha_{\gamma\beta}(\omega_1)|0\rangle}{\omega_{k0} + (\omega_1 - \omega_2) + i2\epsilon} \right], \end{aligned} \quad (2)$$

where the summation now runs over all the excited vibrational states k of the electronic ground state of the molecule. $\alpha_{\alpha\beta}(\omega)$ denotes here the frequency-dependent electronic polarizability, defined as

$$\alpha_{\alpha\beta}(-\omega; \omega) = \frac{1}{\hbar} \sum_{n \neq 0} \left[\frac{\langle 0|\hat{\mu}_\alpha|n\rangle\langle n|\hat{\mu}_\beta|0\rangle}{\omega_{n0} - \omega} + \frac{\langle 0|\hat{\mu}_\beta|n\rangle\langle n|\hat{\mu}_\alpha|0\rangle}{\omega_{n0} + \omega} \right]. \quad (3)$$

Except for the appearance of the finite lifetime of the vibrationally excited states in Eq. (2), the expression for the vibrationally resonant contribution to the second hyperpolarizability is identical with one of the contributing terms to the pure vibrational contribution to the second hyperpolarizability [17,18]. In order to calculate this contribution in an efficient manner, we use perturbation theory and expand the geometry dependence of the electronic polarizability in Eq. (3) in a Taylor series with respect to the normal coordinates \mathbf{Q} :

$$\alpha_{\alpha\beta}(\mathbf{Q}_1, \mathbf{Q}_2, \dots, \mathbf{Q}_N) = \alpha_{\alpha\beta}(\mathbf{R}_{\text{eq}}) + \sum_i \frac{\partial \alpha_{\alpha\beta}}{\partial \mathbf{Q}_i} \mathbf{Q}_i + \dots \quad (4)$$

Representing the vibrational eigenstates as harmonic oscillators, and keeping only the leading order non-vanishing term in the expansion of the polarizability, we obtain the following expression for the resonant contribution to the CARS intensity:

$$\begin{aligned} \gamma_{\alpha\beta\gamma\delta}^{\text{CARS,Res}}(-\omega_\sigma; \omega_1, -\omega_2, \omega_1) \approx & \frac{2}{\hbar} \sum_k \left\{ \left(\frac{\partial \alpha_{\alpha\beta}(\omega_1)}{\partial \mathbf{Q}_k} \right) \left(\frac{\partial \alpha_{\gamma\delta}(\omega_1)}{\partial \mathbf{Q}_k} \right) [\omega_{k0} - (\omega_1 - \omega_2) + i2\epsilon]^{-1} \right. \\ & \left. + \left(\frac{\partial \alpha_{\alpha\delta}(\omega_1)}{\partial \mathbf{Q}_k} \right) \left(\frac{\partial \alpha_{\gamma\beta}(\omega_1)}{\partial \mathbf{Q}_k} \right) [\omega_{k0} + (\omega_1 - \omega_2) + i2\epsilon]^{-1} \right\}. \end{aligned} \quad (5)$$

2.2. Non-resonant Raman scattering

With a common experimental setup of a 90° scattering angle, in which the incident beam (with angular frequency ω) in the Z-direction and polarized along the Y-direction, the differential cross section for Stokes scattering at the harmonic frequency ω_a is given by [19,20]:

$$\frac{d\sigma_a}{d\Omega} = \frac{\hbar}{32\pi^2 \epsilon_0^2 c^4} \frac{(\omega - \omega_a)^4 / \omega_a}{[1 - \exp(-\hbar\omega_a/k_B T)]} \times S_a, \quad (6)$$

where k_B is the Boltzmann constant, T is the temperature, c is the speed of light, and ϵ_0 is the vacuum permittivity. The scattering factor S_a is obtained by considering the general formula:

$$S_a = \left[\overline{(\alpha^{\text{fi}}(\omega))^2} + \frac{7}{45} \beta^2 \right], \quad (7)$$

where $\overline{\alpha^{\text{fi}}(\omega)}$ and β are the isotropic and anisotropic averages in the molecular coordinate system, respectively and defined as

$$\overline{\alpha^{\text{fi}}(\omega)} = \frac{1}{3} \left(\alpha_{xx}^{\text{fi}}(\omega) + \alpha_{yy}^{\text{fi}}(\omega) + \alpha_{zz}^{\text{fi}}(\omega) \right), \quad (8)$$

$$\begin{aligned} \beta^2 = & \frac{1}{2} \left[\left(\alpha_{xx}^{\text{fi}}(\omega) - \alpha_{yy}^{\text{fi}}(\omega) \right)^2 + \left(\alpha_{xx}^{\text{fi}}(\omega) - \alpha_{zz}^{\text{fi}}(\omega) \right)^2 \right. \\ & \left. + \left(\alpha_{yy}^{\text{fi}}(\omega) - \alpha_{zz}^{\text{fi}}(\omega) \right)^2 + 6 \left(\left(\alpha_{xy}^{\text{fi}}(\omega) \right)^2 + \left(\alpha_{xz}^{\text{fi}}(\omega) \right)^2 + \left(\alpha_{yz}^{\text{fi}}(\omega) \right)^2 \right) \right]. \end{aligned} \quad (9)$$

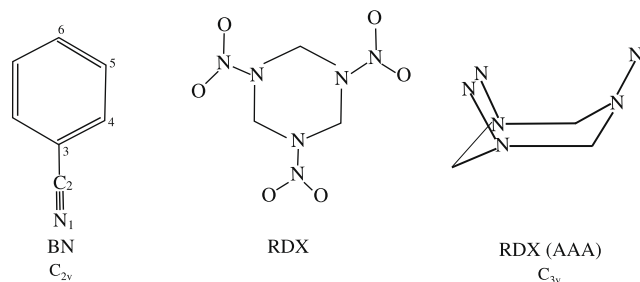


Fig. 1. Molecular structures.

With the initial vibrational state being equal to the ground state ($i = 0$), the polarizabilities $\alpha_{\alpha\beta}^{fi}(\omega)$ are determined in the double harmonic approximation according to the expression:

$$\alpha_{\alpha\beta}^{fi}(\omega) = \sum_a \sqrt{\frac{\hbar}{2\omega_a}} \frac{\partial \alpha_{\alpha\beta}(\omega)}{\partial Q_a}, \quad (10)$$

where ω_a and Q_a are the angular vibrational frequency and coordinate of normal mode a , respectively. Each normal mode gives rise to an oscillating dipole of angular frequency $\omega - \omega_a$. Finally, in the presented Raman spectra, we have converted cross sections from atomic units to units of cm^2/sr with use of the factor $1 \text{ a.u.} = 2.8003 \times 10^{-17} \text{ cm}^2/\text{sr}$.

3. Computational details

We study two molecules in this work; Benzonitrile $\text{C}_7\text{H}_5\text{N}$ (BN) and 1,3,5-trinitro-1,3,5-triazacyclohexane (RDX) $\text{C}_3\text{H}_6\text{N}_6\text{O}_6$, and the calculations of the CARS spectrum and Raman scattering cross sections are performed at room temperature with $T = 300 \text{ K}$. Force fields are determined using the hybrid B3LYP exchange–correlation functional [21–24] together with the double- ζ basis set (cc-pVDZ). The optimized molecular structures of the BN and RDX molecules belong to the point groups C_{2v} and C_{3v} , respectively (see Fig. 1).

In the calculations of the polarizabilities and second hyperpolarizabilities, we use a Hartree–Fock wave function in combination with the cc-pVDZ basis set. The derivatives of the polarizability tensor with respect to nuclear displacements are determined at the B3LYP equilibrium geometries and with the normal coordinates of the mentioned force fields. The geometry optimization and the calculations of force fields have been performed with the

GAUSSIAN program [25], whereas the polarizabilities and second hyperpolarizability calculations have been carried out with the DALTON program [26].

4. Results and discussion

4.1. Test calculations on Benzonitrile (BN)

In order to further benchmark the computational methodology, we choose first to study the benzonitrile molecule which, being a simple aromatic species, shows a high-quality CARS spectrum. The experimental bond distances for the $\text{N}_1\text{—C}_2$, $\text{C}_2\text{—C}_3$, $\text{C}_3\text{—C}_4$, $\text{C}_4\text{—C}_5$ and $\text{C}_5\text{—C}_6$ bonds are 1.159, 1.455, 1.391, 1.393, 1.400 Å, respectively [27], which compares favourably with the optimized structure obtained at the B3LYP/cc-pVDZ level of theory, 1.164, 1.437, 1.406, 1.394 and 1.399 Å, respectively. Since our calculations are concerned with CARS and Raman spectra, it is important to evaluate the quality of the calculated force field, and for this reason we compare our harmonic vibrational frequencies to the experimental fundamental frequencies observed in the non-resonant Raman spectrum reported by Gao et al. [28] and Mrozek et al. [29]. BN has 33 normal modes distributed as twelve modes of A_1 symmetry, eleven of B_2 symmetry, three of A_2 symmetry, and seven of B_1 symmetry. Some of the important calculated harmonic frequency modes, which are active in both the CARS and the Raman spectrum, and the corresponding experimental fundamental frequencies, are presented in Table 1. The experimental fundamental frequencies of the C–H stretch, C–N stretch, C–C stretch, C–H bend and C_{arom} breathing modes are 3065, 2232, 1584, 1162 and 1002 cm^{-1} , respectively. Our corresponding theoretical harmonic frequencies are 3052, 2226, 1570, 1160 and 967 cm^{-1} , respectively (see Table 1). The calculated harmonic frequencies show discrepancies in peak positions of up to 20 cm^{-1} for the overall peaks compared to experimental results, and the origin of these discrepancies are probably due to the approximate nature of the B3LYP functional and medium effects.

The inset in Fig. 2 shows the CARS (upper inset) and non-resonant Raman (lower inset) spectra obtained at the wavelength of 758 nm, covering the wavenumbers between 500 and 3000 cm^{-1} (taken from Ref. [31]). Due to the symmetry of the molecule, only the twelve totally-symmetric modes can contribute to the observed CARS and Raman spectra. It is clear from Fig. 2 that the positions of the spectral features remain the same, while the relative intensities are different in the two spectra. The main difference between them is the peak around 3052 cm^{-1} (Peak 1) which is found

Table 1

Theoretical (harmonic) and experimental^a (fundamental) frequencies (cm^{-1}) and relative^b CARS and Raman intensities for BN and RDX at wavelength 785 and 532 nm, respectively.

| Peak | Frequency | | Mode description | CARS ^b | | Raman ^b | |
|------------|--------------|---------------------------|--------------------------------------|-------------------|--------------|--------------------|--------------|
| | Calculations | Experimental ^a | | Calculations | Experimental | Calculations | Experimental |
| <i>BN</i> | | | | | | | |
| 1 | 3052 | 3065 ^a | C–H, in the plane stretch | 0.8 | 0.8 | 0.3 | 0.1 |
| 2 | 2226 | 2232 | C–N, in the plane stretch | 1.0 | 1.0 | 1.0 | 1.0 |
| 3 | 1570 | 1584 | C–C, in plane stretch | 0.3 | 0.2 | 0.8 | 0.7 |
| 4 | 1160 | 1162 | C–H, in plane bend | 0.2 | 0.2 | 0.6 | 0.8 |
| 5 | 967 | 1002 | C_{arom} , breathing | 0.3 | 0.5 | 0.8 | 1.6 |
| <i>RDX</i> | | | | | | | |
| 1 | 1340 | 1316 | C–H, in the plane stretch | 1.0 | 0.8 | 0.6 | 0.6 |
| 2 | 1284 | 1275 | C–N, in the plane stretch | 0.3 | 0.6 | 0.5 | 0.5 |
| 3 | 1232 | 1222 | C–N, bend out of plane | 0.1 | 0.6 | 0.1 | 0.7 |
| 4 | 890 | 890 | Ring atoms, breathing | 1.0 | 1.0 | 1.0 | 1.0 |
| 5 | 860 | 853 | Ring atoms C–N, stretch | 0.2 | 0.4 | 0.5 | 0.4 |

^a 'a' is taken from Refs. [28,29,35], respectively.

^b Theoretical and experimental relative intensities for BN and RDX are obtained by normalizing with respect to Peaks 2 and 4, respectively.

to be the second strongest in the CARS spectrum, while being very weak in the Raman spectrum. There are only three symmetric modes that contribute strongly to the CARS spectrum, namely the two stretch symmetric modes C–H (Peak 1), C–N (Peak 2) and one symmetric breathing mode C_{arom} (Peak 5) in Fig. 2. On the other hand, the lower inset spectrum reveals that, in the non-resonant Raman case, there are four symmetric modes that contribute strongly to the Raman spectrum, namely the C–N (Peak 2), C–C (Peak 3), C–H (Peak 4) and C_{arom} (Peak 5) (see Table 1). The theoretical CARS and Raman spectra as obtained at the HF/cc-pVDZ level of theory at the wavelength of 758 nm are presented for wavenumbers between 500 and 3000 cm^{-1} in Fig. 2. We note that, just as in the experimental spectrum, the scattering intensities are

dominant for most of these discussed symmetric modes. The perhaps most striking difference between the CARS and non-resonant Raman spectra is that the peak at 3052 cm^{-1} (Peak 1), seen as the second strongest in the CARS spectrum, is among the weakest in the Raman spectrum, and it is of course pleasing to note that this change in the fingerprint of BN is well reproduced in the theoretical calculation (see Fig. 2). The calculated and experimental relative intensities of the CARS and Raman spectra are presented in Table 1. The prediction of the relative CARS intensities for the same peaks shows a compelling overall agreement between the theoretical and experimental spectra. It is clear that, with applications of stand-off detection in mind, the molecular fingerprint changes quite dramatically between the CARS and Raman signals.

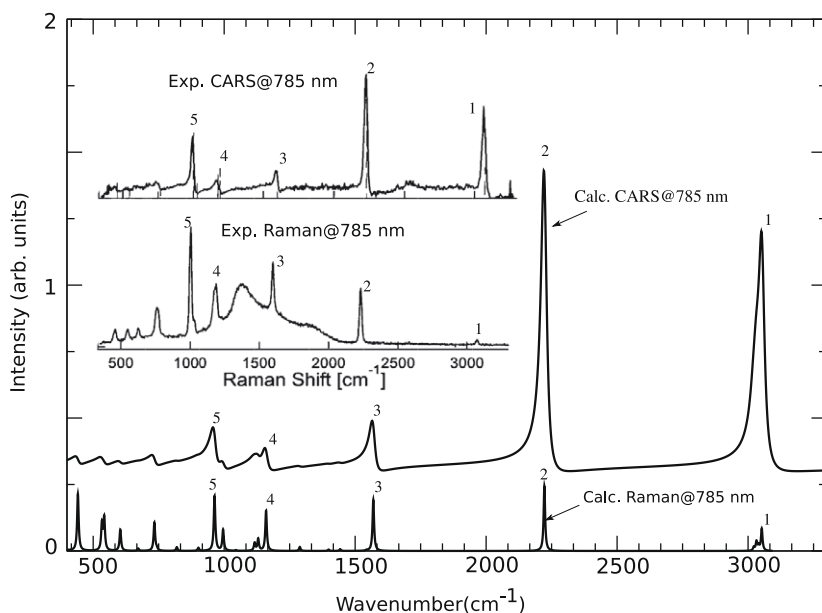


Fig. 2. Calculated CARS and non-resonant Raman spectra for Benzonitrile at 785 nm. The inset shows the experimental CARS and non-resonant Raman spectra, which is taken from Ref. [31].

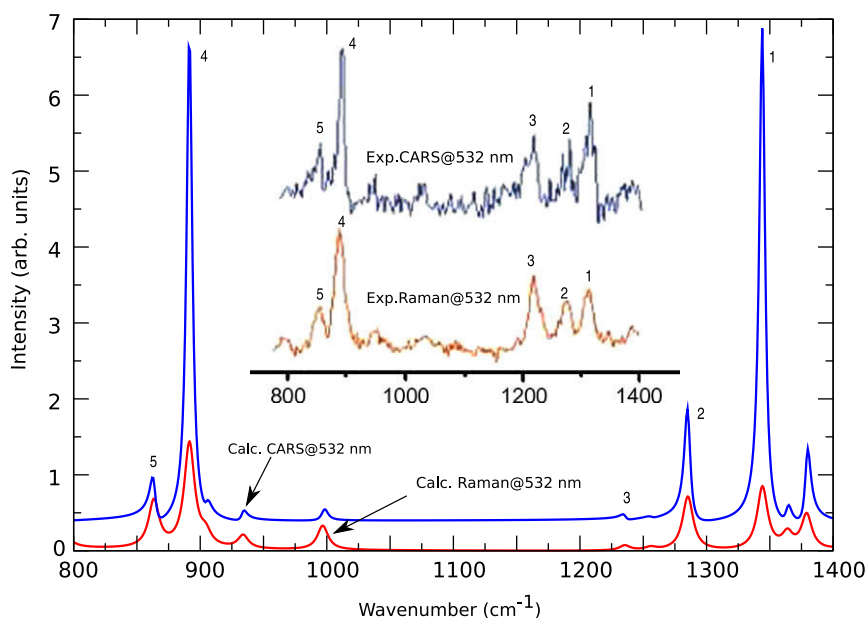


Fig. 3. Calculated CARS and non-resonant Raman spectra for RDX at 532 nm. The inset shows the experimental CARS and non-resonant Raman spectra, which is taken from Ref. [35].

4.2. 1,3,5-trinitro-1,3,5-triazacyclohexane (RDX)

Based on B3LYP calculations, six molecular conformations of 1,3,5-trinitro-1,3,5-triazacyclohexane (RDX) were reported in Ref. [32]. The conformations differ by the arrangement of the nitro groups relative to the ring atoms of the RDX molecule. It was shown that the most stable conformer in gas phase was the one belonging to the C_{3v} point group, namely the AAA conformer [32–34]. The spectra presented in the present work are obtained for this conformer (see Fig. 1). In fact, test calculations on a different conformers indicate significant differences in the spectra, deteriorating the agreement with experiment, indicating that CARS spectra indeed can distinguish conformers of molecules like RDX (see Fig. 4). The calculated and experimental frequencies of the Raman and CARS signals are shown in Table 1. The experimental fundamental frequencies of the C–H stretch, C–N stretch, C–N bend, ring atom breathing modes and C–N ring atom stretch modes are 1316, 1275, 1222, 890 and 853 cm^{-1} , respectively. Our corresponding theoretical harmonic frequencies are 1340, 1284, 1232, 890 and 860 cm^{-1} , respectively (see Table 1). There are discrepancies in peak position of up to 25 cm^{-1} for the overall peaks compared to experimental results and, these discrepancies are predominantly due to the neglect of anharmonicities in the true potential. We can thus conclude that our theoretical harmonic force field is quite accurate and that demonstrates the reliability of the B3LYP functional in frequency calculations [19,20,34].

In Fig. 3 we present the calculated non-resonant Raman differential cross sections and CARS spectrum for RDX in gas phase for the frequency region 800–1400 cm^{-1} at a wavelength of 532 nm. The experimental CARS (upper) and Raman (lower) spectrum for RDX was reported and analyzed in the work of Portnov et al. [35] and are shown as insets in Fig. 3. We note, as in the spectra for BN, that the positions of the CARS spectrum is consistent with the Raman spectrum while the relative intensities are not. The experimental Raman and CARS fingerprints of RDX consist of one strong peak at 890 cm^{-1} (Peak 4) and four medium strong peak at 853 (Peak 5), 1222 (Peak 3), 1275 (Peak 2) and 1316 (Peak 1)

cm^{-1} for Raman, while for CARS there are two strong signals at 890 (Peak 4) and 1316 (Peak 1) cm^{-1} and three medium strong peaks at 853 (Peak 1), 1222 (Peak 3) and 1275 (Peak 2) cm^{-1} . With respect to the prediction of the intensities for these peaks, the agreement between the theoretical and experimental spectra is satisfactory. However, it is fair to say that the theoretical CARS spectrum around 1222 (Peak 3) cm^{-1} is, just as in the non-resonant Raman case, not too accurate. In the two cases, this region acquires too low intensity as compared to the experimental spectrum.

5. Conclusion

We have studied the coherent anti-Stokes Raman scattering (CARS) spectrum of the 1,3,5-trinitro-1,3,5-triazacyclohexane (RDX) $\text{C}_3\text{H}_6\text{N}_6\text{O}_6$ molecule. We have compared the calculated spectra with the highly resolved CARS spectrum for the benzonitrile $\text{C}_7\text{H}_5\text{N}$ (BN) molecule, and also performed comparative calculations of the non-resonant Raman spectra of the two molecules. The calculated spectra reveal that all the symmetric modes contribute strongly to the spectra of the studied molecules, but quite differently so for the CARS and Raman spectra. A motivation for our interest in this field is the use of CARS spectroscopy for stand-off detection of gaseous samples at ultra-low concentrations. In such applications, the CARS spectra can function as fingerprints of the explored substances. The use of the resonant CARS conditions implies an overall increase of the intensity by several orders of magnitude over normal Raman and gives the possibility to improve the accuracy in the identification process by considering the diversity of the fingerprints obtained by this technique. Complementing earlier theoretical modelling tools for conventional Raman spectra, with our methodological development for both resonant Raman [19,30] and CARS [12], we have at our disposal of a powerful modelling toolbox for the three different Raman techniques, that all have complementary merits and limitations in order to disclose the content of foreign unknown substances, and theory may thus be a valuable aid in the technical design of such measurements.

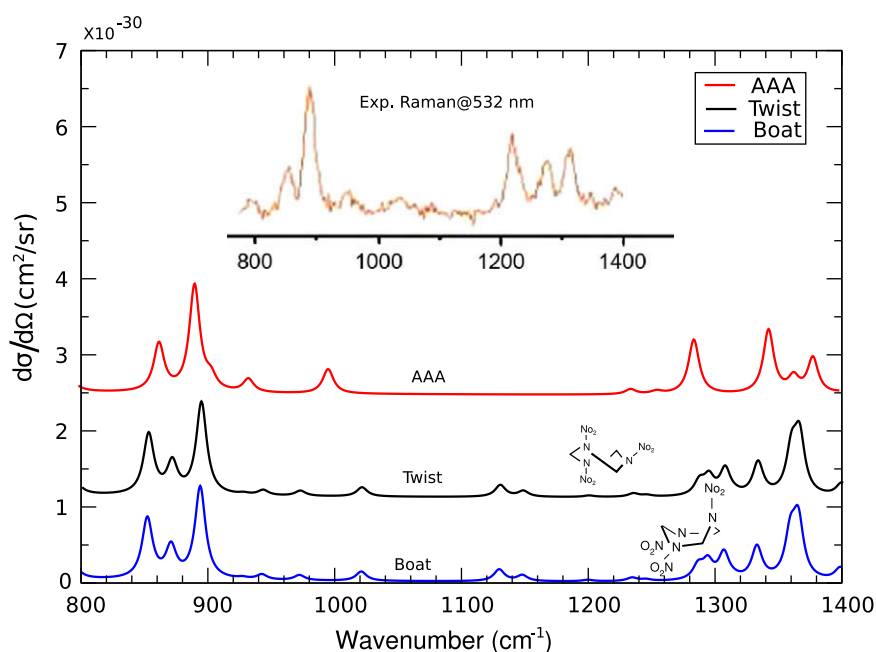


Fig. 4. Calculated non-resonant Raman spectra for RDX at 532 nm for different conformations. The inset shows the experimental non-resonant Raman spectra, which is taken from Ref. [35]. The spectra have been broadened with a Lorentzian having a width of 20 cm^{-1} .

Acknowledgments

This work was supported by a grant from the Swedish Infrastructure Committee (SNIC) for the project 'Multiphysics Modeling of Molecular Materials', SNIC 023/07-18. This work has also received support from the Norwegian Research Council through a Centre of Excellence Grant (Grant No. 179568/V30) and a VIBRON Grant (Grant No. 177558/V30), as well as through a grant of computer time from the Norwegian Supercomputing Program.

References

- [1] J. Cheng, A. Volkmer, X. Sunney, *J. Opt. Soc. Am.* 19 (2002) 1363.
- [2] L.C. Evans, S.X. Xie, *Annu. Rev. Anal. Chem.* 1 (2008) 883.
- [3] Z. Chi, S. Asher, *J. Phys. Chem. B* 102 (1998) 9595.
- [4] W.F. Schneider, *Non-Linear Raman Spectroscopy and its Chemical Applications*, D. Reidel Publishing Company, 1982.
- [5] Z.K. Tang, J.P. Zhai, Y.Y. Tong, X.J. Hu, R. Saito, Y.J. Feng, P. Sheng, *Phys. Rev. Lett.* 101 (2008) 047402.
- [6] M. Rybachuk, A. Hu, J.M. Bell, *Appl. Phys. Lett.* 93 (2008).
- [7] S. Shim, C.M. Stuart, R.A. Mathies, *Chem. Phys. Chem.* 9 (2008) 697.
- [8] M. Husanu, M. Baibarac, N. Preda, I. Baltog, *J. Optoelectron. Adv. Mater.* 10 (2008) 1722.
- [9] A. Blanco, L.C. Pacheco-Londoño, A.J. Peña-Quevedo, S.P. Hernández-Rivera, *Proc. SPIE* 6217 (2006) 621737.
- [10] A.L. Carreira, L.M. Horovitz, *Non-Linear Raman Spectroscopy and its Chemical Applications*, D. Reidel Publishing Company, England, 1982.
- [11] M.W. Tolles, W.J. Nibler, R.J. McDonald, B.A. Harvey, *J. Appl. Spectrosc.* 31 (1977).
- [12] H. Ågren, P. Jørgensen, S. Coriani, *Phys. Chem. Chem. Phys.* 11 (2009) 2293.
- [13] A.J. Thorvaldsen, K. Ruud, K. Kristensen, P. Jørgensen, S. Coriani, *J. Chem. Phys.* 129 (2008) 214108.
- [14] S. Mukamel, *Principles of Nonlinear Optical Spectroscopy*, Oxford University Press, New York, 1995.
- [15] P. Norman, K. Ruud, *Nonlinear Optical Properties of Matter: From Molecules to Condensed Phases, Microscopic Theory of Nonlinear Optics*, Kluwer, Dordrecht, 2006.
- [16] A.J. Thorvaldsen, K. Ruud, M. Jaszuński, *J. Phys. Chem.* 112 (2008) 11942.
- [17] D.M. Bishop, B. Kirtman, *J. Chem. Phys.* 95 (1991) 2646.
- [18] D.M. Bishop, B. Kirtman, *J. Chem. Phys.* 97 (1992) 5255.
- [19] A. Mohammed, H. Ågren, P. Norman, *Phys. Chem. Chem. Phys.* 11 (2009) 4539.
- [20] A. Mohammed, B. Minaev, H. Ågren, L. Mikael, P. Norman, *Chem. Phys. Lett.* 481 (2009) 209.
- [21] A.D. Becke, *J. Chem. Phys.* 98 (1993) 5648.
- [22] C.T. Lee, W.T. Yang, R.G. Parr, *Phys. Rev. B* 37 (1988) 785.
- [23] B. Miehlich, A. Savin, H. Stoll, H. Preuss, *Chem. Phys. Lett.* 157 (1989) 200.
- [24] S.H. Vosko, L. Wilk, M. Nusair, *J. Chem. Phys.* 58 (1980) 1200.
- [25] M.J. Frisch et al., *GAUSSIAN 98*, Gaussian Inc., Pittsburgh PA. <<http://www.gaussian.com>>, 1998.
- [26] DALTON, a molecular electronic structure program, release 2.0. <<http://www.kjemi.uio.no/software/dalton/dalton.html>>, 2005.
- [27] B. Bak, D. Christensen, B.W. Dixon, L. Hansen-Nygaard, J. Rastrup-Andersen, *J. Chem. Phys.* 37 (1962) 2027.
- [28] X. Gao, J.P. Davies, M.J. Weaver, *J. Phys. Chem.* 94 (1990) 6858.
- [29] M.F. Mrozek, S.A. Wasileski, M.J. Weaver, *J. Am. Chem. Soc.* 123 (2001) 12817.
- [30] A. Mohammed, H. Ågren, P. Norman, *Chem. Phys. Lett.* 468 (2009) 119.
- [31] T.W. Kee, M.T. Cicerone, *Opt. Lett.* 29 (2004) 23.
- [32] T. Vladimiroff, M.B. Rice, *J. Phys. Chem. A* 106 (2002) 10437.
- [33] B.M. Rice, F.C. Chabalowski, *J. Phys. Chem. A* 101 (1997) 8720.
- [34] N. Harris, K. Lammertsma, *J. Am. Chem. Soc.* 119 (1997) 6583.
- [35] A. Portnov, S. Rosenwaks, I. Bar, *Appl. Phys. Lett.* 93 (2008).